Bull Earthquake Eng (2008) 6:585–605
DOI 10.1007/s10518-008-9079-0

ORIGINAL RESEARCH PAPER

Centrifuge modelling of normal fault–foundation interaction

M. F. Bransby · M. C. R. Davies · A. El. Nahas

Received: 22 October 2007 / Accepted: 16 July 2008 / Published online: 28 August 2008

Abstract Earthquake fault ruptures may emerge at the ground surface causing large differential movements. When fault ruptures emerge at or adjacent to the position of existing foundations, significant damage can be caused. However, the study of recent faulting events revealed that in some circumstances the fault-rupture emergence is deflected by the presence of buildings leaving the buildings intact. A centrifuge modelling study has been conducted to investigate how normal faults interact with strip foundations which run parallel to the strike direction. The study confirms that fault rupture may be deviated by the presence of the foundation so that the foundation is protected from the most serious differential movements. However, whilst the fault propagates to the soil surface the foundation has to withstand initial movements before the final fault rupture emergence mechanism is activated. The centrifuge results suggest that it is the bearing pressure of the foundation which causes the deviation of the fault rather than the kinematic restraint of the foundation. The interaction between the earthquake fault and the shallow foundation depends on the foundation bearing pressure, foundation width, soil depth and position of the fault relative to the foundation and these aspects should be considered in design. Results from the tests are used to validate a series of finite element analyses as reported in an accompanying paper.

Keywords Centrifuge modelling · Earthquake fault rupture · Shallow foundations

1 Introduction

During earthquakes, both transient ground shaking and permanent ground deformation are produced. To date, most research has concentrated on the performance of infrastructure when subject to transient ground shaking due to the large spatial extent of this excitation. However, the permanent ground deformation caused by faulting is a serious hazard to the serviceability of infrastructure (e.g. Bray 2001; O'Rourke 2003). Detailed study of earthquakes (particularly

M. F. Bransby (✉) · M. C. R. Davies · A. El. Nahas
Division of Civil Engineering, University of Dundee, Nethergate, Dundee DD1 4HN, UK
e-mail: m.f.bransby@dundee.ac.uk

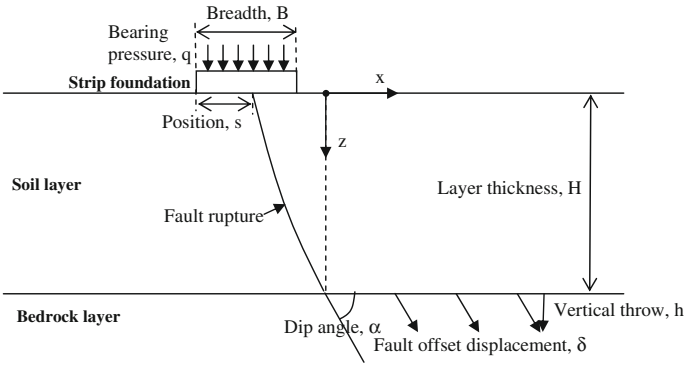

Fig. 1 Geometry of normal fault rupture emergence adjacent to a shallow foundation

those in Turkey and Taiwan in 1999) has revealed that, in particular, there is complex interaction between earthquake faults and buildings supported by shallow foundations. In some cases the buildings appeared able to divert the earthquake fault rupture emergence away from the buildings (Niccum et al. 1976; Ulusay et al. 2002; Anastasopoulos and Gazetas 2007a,b; Faccioli et al. 2008) and thereby suggest that it is possible for shallow foundations to be designed to withstand nearby earthquake faulting.

This paper reports a study using centrifuge modelling to investigate the performance of shallow foundations resting on shallow soil layers subject to normal dip-slip faulting. Centrifuge modelling was used to allowed detailed examination of the factors that affect the foundation–fault interaction in a controlled environment, with soil at appropriate effective stress levels. In addition, the data was used for validation of numerical work reported elsewhere (e.g. Anastasopoulos et al. 2008) and to inform design (Pecker et al. 2008).

The work formed part of a study comprising of field testing, numerical modelling and physical modelling carried out during the EU-funded QUAKER project. Additional insight was gained of fault–foundation interaction by integrating findings from the different research methods and many of these finding are reported in accompanying papers (e.g. Faccioli et al. 2008; Anastasopoulos et al. 2008; Pecker et al. 2008).

The centrifuge test series comprised of free-field tests (without foundations) which could be compared with those with foundations present for examination of interaction effects. Also included was a parametric study designed to investigate the effect of foundation position, bearing pressure and breadth on the fault–foundation interaction.

This paper will concentrate on the behaviour of normal dip-slip faults with a 60° dip angle propagating through a shallow soil layer. The foundation and soil geometry is shown schematically in Fig. 1. A dip-slip normal fault rupture is propagated by the downwards displacement of the bedrock at 60° to the horizontal. In the free-field case a fault will propagate through the soil layer and emerge at the soil surface if there is sufficient fault displacement. The undisplaced side of the fault is denoted as the foot wall, while the deforming block is called the hanging wall. A surface footing of breadth B with applied vertical pressure, q, rests on the soil surface with its foot wall edge a distance s from the position of the emergence of a fault for the free-field case.

A 60° dip angle was selected to agree with common field conditions, and the soil response was modelled to be drained and quasi-static agreeing with findings from case histories (Faccioli et al. 2008; Anastasopoulos and Gazetas 2007a).

2 Background

Modelling has been carried out previously to investigate the propagation of dip-slip earthquake faults through soil layers without foundations, using physical model testing (e.g. Roth et al. 1981; Cole and Lade 1984; Bray 1990; Lazarte and Bray 1996) and numerical modelling (e.g. Bray et al. 1994; Roth et al. 1982). General findings include the realisation that both normal and reverse fault propagation through soil is a progressive event with the final emergence of the fault rupture (if it occurs) dependent on the soil layer depth, the soil properties (particularly angle of dilation), dip angle and fault mode. These findings have been supported by field evidence (e.g. Lade et al. 1984; Bray 1990; Scott and Schoustra 1974).

Considerably less research has investigated the interaction between shallow foundations and faulting events and most findings have resulted from investigation of field events (e.g. Niccum et al. 1976; Bray 2001; Ulusay et al. 2002; Pamuk et al. 2005). In terms of modelling, Berill (1983) used upper bound plasticity to suggest the interaction between shallow foundations for strike-slip faulting events in undrained soil. This approach has recently been extended to dip-slip faults in undrained materials (Yilmaz and Paolucci 2006). Bray and his co-workers have investigated aspects of the interaction behaviour with combinations of numerical modelling (e.g. Bray 2001), field investigations and laboratory scale model testing (Lazarte 1996; Lazarte and Bray 1996), but most of this work was conducted for undrained ('cohesive') soils.

To date, no physical modelling has been performed to investigate fault–foundation interaction for drained conditions where the effective stress state of the soil is equivalent to that in the field event. This is important because Cole and Lade (1984) demonstrated that it is the dilation angle which controls significantly the position of the fault propagation, and dilation angle (for a given relative density) is dependent on effective stress (e.g. Bolton 1986). Centrifuge modelling, where a reduced-scale sample is subject to an elevated acceleration field, is an effective tool for correctly modelling the effective stress profile of a controlled, scaled soil sample (e.g. Schofield 1980) and this technique is used here.

3 Experimental methods and apparatus

3.1 Model geometry and apparatus

A schematic view of the boundary value problem investigated in the centrifuge model tests is shown in Fig. 2a. For all tests reported here, a normal fault of dip angle 60° was propagated through a dry sand layer of depth, H = 25 m (at prototype scale) in a quasi-static, drained manner. Tests were conducted at 115 times Earth's gravity in the Dundee University beam centrifuge so that prototype dimensions were 115 times greater than the model, but the stress levels in the model and prototype were equal. For more details of centrifuge scaling laws see Schofield (1980) and Muir Wood (2004).

The apparatus is shown in Fig. 2b and c. The apparatus was contained within a centrifuge strong box of internal dimensions 800 × 500 mm (in plan) and 500 mm deep which had a front and back face constructed from Perspex. A split box was constructed within this strongbox of internal dimensions 655.9 mm (wide) × 500 mm (broad) × 220 mm (deep) which contained the soil (see Fig. 2b and c). For the tests here conducted at 115 g, this represents a soil depth of 25 m and a zone 79 m by 57.5 m in plan. Aluminium blocks were used to support rigidly the soil on the footwall (left hand) side of the box. A rigidly translating base and wall (shown shaded in Fig. 2b) on the hanging wall (right hand side) of the soil sample provided the

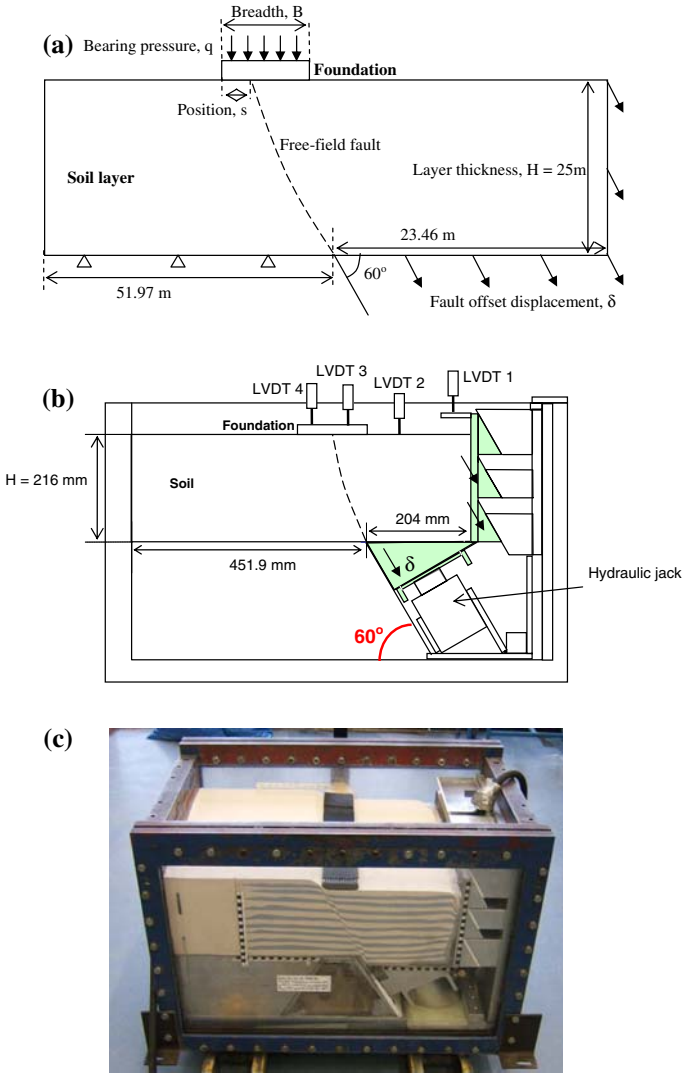

Fig. 2 The centrifuge apparatus. (**a**) Schematic of the test boundary conditions during normal faulting (not to scale). (**b**) Schematic of the centrifuge apparatus. (**c**) Photograph of centrifuge apparatus (after centrifuge test 22)

displacement boundary condition. The displacing rigid hanging wall base and wall section was supported by a pair of hydraulic jacks which were used for actuation. By pumping oil into the jacks, the block was lifted and a reverse fault was activated; by removing oil from the jacks, the block moved downwards and a normal fault was activated. The maximum stroke length achievable using this apparatus in the normal faulting mode was 26.4 mm, representing a 3.04 m fault displacement (δ) at prototype scale. To ensure that the apparatus gave a fixed dip angle, a linear bearing was placed on the left side of this base block (supported by the rigid aluminium blocks supporting the footwall) and an additional three bearings were placed on aluminium blocks connected to the displacing (hanging wall) side wall. These bearings

were all inclined at 30° to the vertical giving a dip angle of 60°. All edges of the split box were lined with sandpaper to ensure that fully rough boundary conditions were modelled.

3.2 Sample preparation

All tests were conducted with dry sand to ensure drained conditions. Fontainebleau sand was used because of its known properties and previous use by researchers. This is a uniform fine silica sand with $d_{50} = 0.3$ mm, $\rho_{max} = 1703$ kg/m^3, $\rho_{min} = 1440$ kg/m^3 (Gaudin 2002).

The soil was prepared by dry pluviation to give a target relative density, $D_r = 60\%$. This corresponds to a unit weight, $\gamma = 15.67$ kN/m^3. Coloured sand layers were placed in close proximity to the front face to allow visual detection of shear planes. The sand used for these layers was Fontainebleau sand dyed with blue ink and this was pluviated to form approximately 10 mm thick layers. Direct shear tests were conducted on samples with $D_r = 60\%$ which gave $\phi'_{pk} = 35°$ and $\psi' = 6°$ at the effective stress at the mid-depth of the sand layer ($\sigma'_v = 15.67$ kN/m^3 $\times$ 12.5 m $= 196$ kN/m^2) in the centrifuge tests and prototype.

The foundations were constructed from either steel or aluminium and were of breadth, B/115 (typically 87 mm for a 10 m wide foundation at full scale) and thickness 10 mm. All were of length, L = 500 mm (the width of the soil container) giving plane strain conditions and had rough bases. The foundation bearing pressure was achieved by controlling the self-weight of the foundation. Steel foundations gave bearing pressure, q = 91 kN/m^2 and an aluminium foundation gave a bearing pressure, q = 37 kN/m^2. The foundations were placed directly on the soil surface in the appropriate position from the fault, ensuring that they were parallel to the strike of the fault and that one side of the foundation was in close proximity to the Perspex front face. Markers were placed on this visible foundation face to facilitate later digital image analysis.

3.3 Model instrumentation

Point measurement of displacement was achieved using four linearly variable differential transformers (LVDT) positioned as shown in Fig. 2b which were logged throughout the tests. One of the LVDTs was placed on the displacing rigid apparatus and gave direct measurement of the vertical component of the fault displacement (h) and this was used to monitor the progress of the fault actuation during testing. Additional LVDTs allowed measurement of vertical movements of the soil surface and/or the foundation.

Measurement of soil displacement fields and foundation movements was achieved by the use of digital image analysis. Digital images of the soil sample were captured through the Perspex front face using a Canon S45 digital camera placed on the gondola of the centrifuge. As the faulting tests proceeded, a series of up to 80 digital images were collected each corresponding to a different fault displacement. The robust optical flow programme, Geo-PIV, written by White et al. (2003) was then used to obtain soil displacement measurements by comparison of pairs or sequences of the digital images captured in flight. Post processing in the Matlab environment allowed examination of displacement and strain fields.

3.4 Centrifuge test sequence

Once the target centrifuge acceleration (115g) was reached, an initial digital image was captured. Faulting was initiated by letting out oil from the hydraulic cylinder. Digital images were captured for increasing fault movements until the maximum fault offset was achieved at which time the centrifuge was stopped. Digital images were taken of the reverse side of

Table 1 Centrifuge testing programme

Test identifier	Footing breadth (m)	Bearing pressure (kPa)	Relative density [Dr (%)]	Fault position [s (s/B)]
12	–	–	60.2	–
14	10	91	62.5	3.0 m(0.3)
15	10	37	59.2	3.1 m(0.31)
18	10	91	63.7	8.5 m(0.85)
20	25	91	56.0	10.9 m(0.44)
22	9.43 (flexible)	91	55.7	3.2 m(0.34)

the strongbox and of the soil surface after the test to ensure that the soil deformation was in plane strain.

The programme of model tests is shown in Table 1. Following a free-field test (H = 25 m), five further foundation tests allowed investigation of the effect of bearing pressure (q), foundation breadth (B), foundation position (s) and foundation flexibility. The results of the tests are presented below at prototype scale unless specified otherwise.

4 Results

4.1 Free-field conditions (test 12)

Before conducting the fault–footing interaction tests, it was important to investigate the manner of normal fault propagation for the free-field case. Consequently, test 12 investigated a dry sand layer of depth, H = 25 m and relative density, $D_r \approx 60\%$ which was used in the later fault–foundation interaction tests.

A selection of the digital images captured during tests 12 are shown in Fig. 3. Figure 3a shows the image for a vertical component of fault movement (throw), h = 0.48 m (h = 4.2 mm at model scale). The hanging wall has moved downwards only a small distance and there is no localisation visible in the image. However, by a displacement, h = 0.8 m (Fig. 3b) first a very steep, short vertical localisation ('S1' in Fig. 3b) and then a longer localisation ('S2' in Fig. 3b) is mobilised approximately $3/5^{th}$ to the soil surface from the base. This is shown in more detail in Fig. 4a. By a displacement, h = 1.15 m (Fig. 3c) both S1 and the top section of S2 have become inactive, and a new 'final' localisation ('S3' in Fig. 3c) is active and has propagated to the soil surface. This fault continues to be active for larger fault displacements (Fig. 3d). A close up of the final fault near the bedrock discontinuity is shown in Figure 4b.

Soil deformation mechanisms deduced from image analysis at different stages of fault propagation are shown in Fig. 5. Both incremental soil displacement vectors and contours of maximum shear strain are presented. Figure 5a shows that the initial (i.e. small fault movement) deformation field is very diffuse with no localisation occurring. This is confirmed with a plot of the measured surface settlement profile shown in Fig. 6. For fault movements, h ≤ 0.8 m, the soil surface deforms with a continuous profile as the fault has not propagated to the surface. Figure 5b shows that for larger fault movements (when S2 is active) there is more localisation but no emergence at the surface (Fig. 6). Finally, on fault outcropping (when h ≤ 1.01 m), there is a strong discontinuity of surface settlement (Fig. 6) and soil deformation (Fig. 5c) as shear plane S3 propagates up to the soil surface (Fig. 3c).

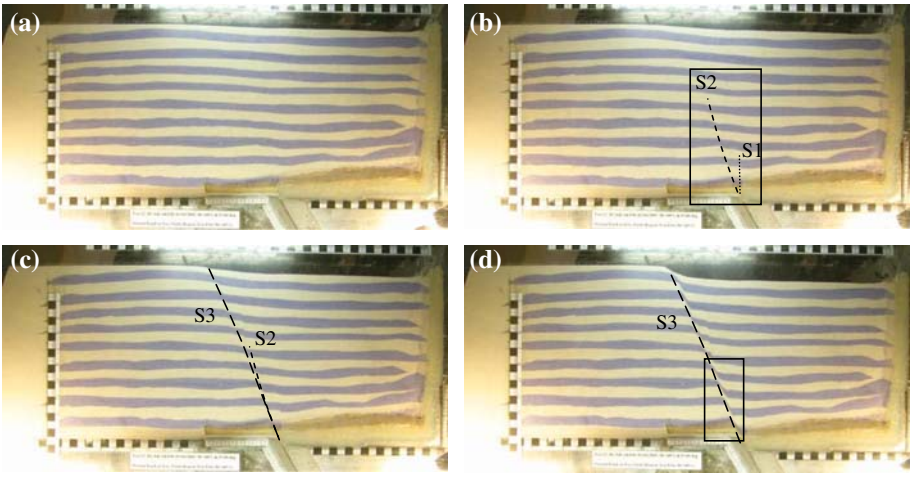

Fig. 3 Photographs taken during normal fault propagation: test 12. (**a**) Fault throw, h = 0.48 m (h_{model} = 4.2 mm). (**b**) h = 0.80 m (h_{model} = 6.9 mm). (**c**) h = 1.15 m (h_{model} = 10.0 mm). (**d**) h = 2.16 m (h_{model} = 18.8 mm)

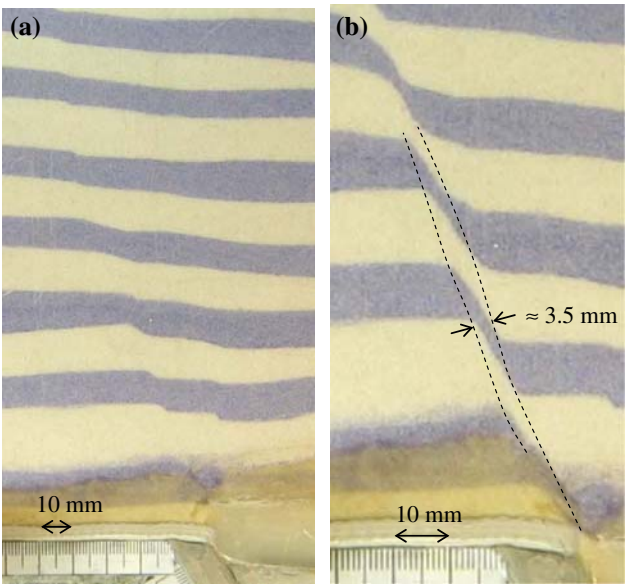

Fig. 4 Enlargements of selected portions of images captured during test 12. (**a**) Close up of rectangular zone shown in Figure 3b. (**b**) Close up of zone highlighted in Fig. 3d

The surface displacement profiles (Fig. 6) and the shear strain contour plot on Fig. 5c reveal that once the discontinuity had reached the soil surface, there was no further deformation of the soil surface outside the shear plane: the soil on the foot wall remains rigid and stationary; the soil on the hanging wall translates rigidly.

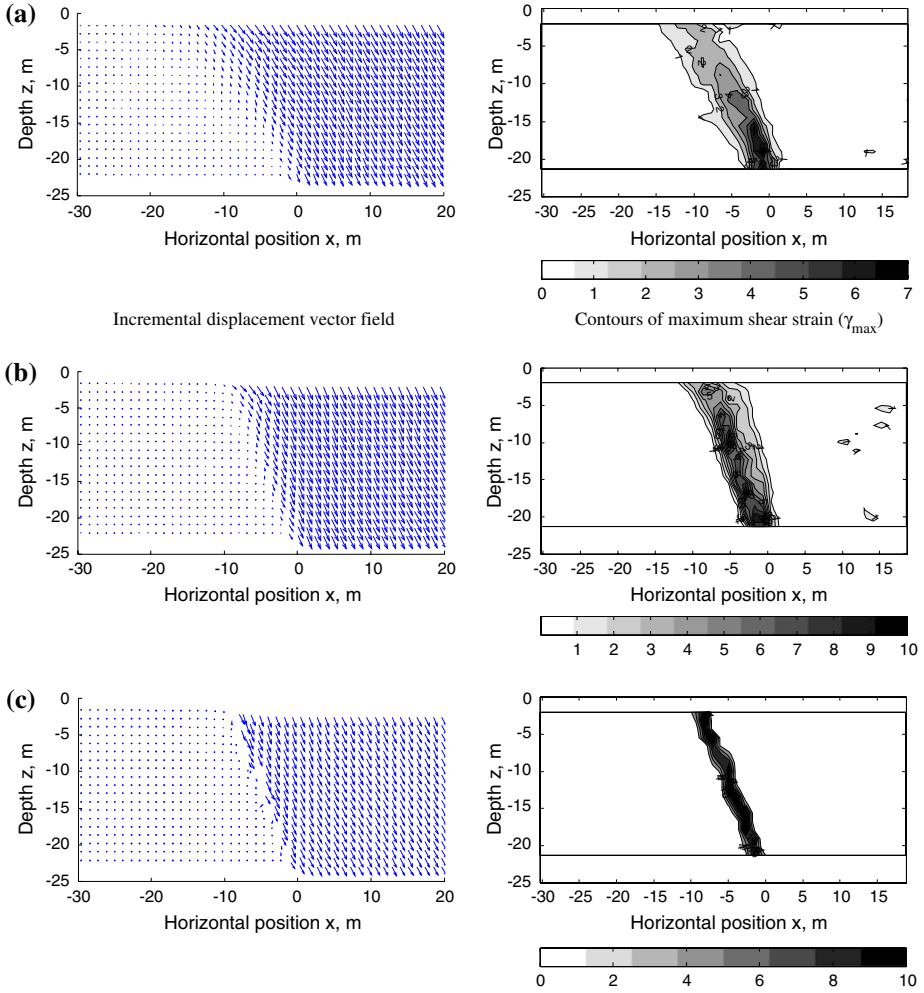

Fig. 5 Incremental soil displacement vectors and shear strain contours at different stages of fault-rupture propagation for a free-field normal fault (test 12). (**a**) Fault throw, h = 0 to 0.174 m (Δh = 0.174 m) Δh/H = 0.7% (**b**) h = 0.48 to 0.67 m (Δh = 0.19 m) (**c**) h = 1.01 to 1.15 m (Δh = 0.14 m)

The results demonstrate that the fault propagation is progressive due to the ductility of the soil as pointed out by previous researchers (e.g. Cole and Lade 1984; Roth et al. 1982; Bray et al. 1994). The initial localisations ('S1' and possibly 'S2') are likely to be due to high dilation at small shear strains on initial deformation of the soil layer (e.g. Muir Wood and Stone 1994; White et al. 1994). The final failure mechanism ('S3') has a single displacement discontinuity (fault) with a dip angle (67°), slightly steeper than that applied at the base of the soil layer. To mobilise this to the soil surface required a fault throw, h = 1.01 m (4% of the soil height) and the fault rupture emerged 9.8 m (85 mm model scale) to the foot wall side of the basement fault.

The expanded view of the shear localisation shown in Fig. 4b reveals that the shear band thickness is approximately 3.5 mm at model scale. This corresponds to 11.67d_{50} agreeing with

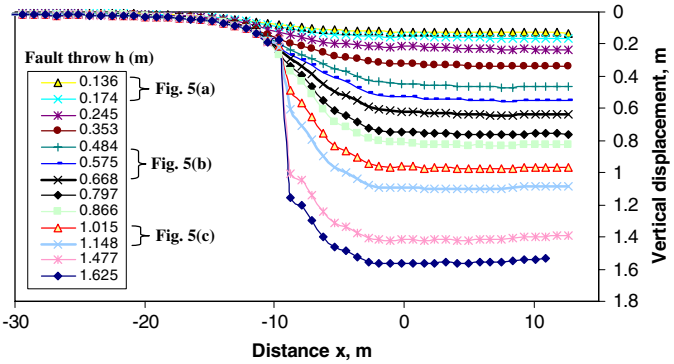

Fig. 6 Vertical displacement profile near the soil surface (at depth, z = 0.9 m) for increasing fault throw (h). Free-field fault (test 12)

the results of previous researchers (e.g. Scarpelli and Wood 1982; Muhlhaus and Vardoulakis 1987; Muir Wood 2002). Note that this corresponds to a shear band thickness of approximately 400 mm at full scale. It should also be noted that previous researchers have suggested that a relative displacement across a displacement discontinuity of between $100d_{50}$ (Scarpelli and Wood 1982), $120d_{50}$ (Vardoulakis et al. 1981) and $176d_{50}$ (Stone and Muir Wood 1992) is required to move from peak strength (with associated dilation) to a critical state (with zero dilation). For the particle size used in these experiments, this corresponds to a relative displacement between 30 and 52.8 mm, suggesting that the model scale throw, $h_{model} = 18.8$ mm (relative displacement, $\delta_{model} = 21.7$ mm) for Fig. 4b may not have generated critical state conditions.

4.2 Fault-rupture–footing interaction: base case with B = 10 m; q = 91 kPa, s = 3.0 m (test 14)

A foundation of breadth, B = 10 m and bearing pressure, q = 91 kPa was used as the base condition (test 14; Table 1). These parameters were selected as typical of those expected for an 8-storey building with a raft foundation. The foundation was placed on the soil surface so that the free-field fault would have emerged at a distance, s = 3.0 m (s/B = 0.3) to the right of the left hand (foot wall) edge of the foundation (see Fig. 7a).

Four of the digital images captured during this fault–footing interaction test are shown in Fig. 7. For small fault displacements (Fig. 7a) there is no localisation. In Fig. 7a the foundation can be seen on the top surface of the soil and the free-field fault position is indicated. For larger fault displacements (h = 0.48 m in Fig. 7b) an initial steep localisation has formed similar to that observed in the free-field test. Note, however that there is no observable vertical slip plane and 'S1' for this test corresponds to 'S2' for the free-field test. By a fault displacement, h = 0.99 m (Fig. 7c) the shear plane 'S1' has almost reached half way up the soil surface and a second shear plane ('S2' Fig. 7c) has propagated from the left hand edge of the foundation downwards to a depth of about 0.5 B. Note, at this displacement the main fault ('S3' in Fig. 3c) had emerged at the ground surface in the free field test. For the final image ($h \approx 2$ m), the failure mechanism consists of a single discontinuity on the line of 'S2' (Fig. 7d) and 'S1' has become inactive. The calculated soil displacements for the final mechanism (when $h \approx 2$ m) is shown on Fig. 8 and demonstrates that there are negligible deformation outside the shear plane once the final mechanism forms.

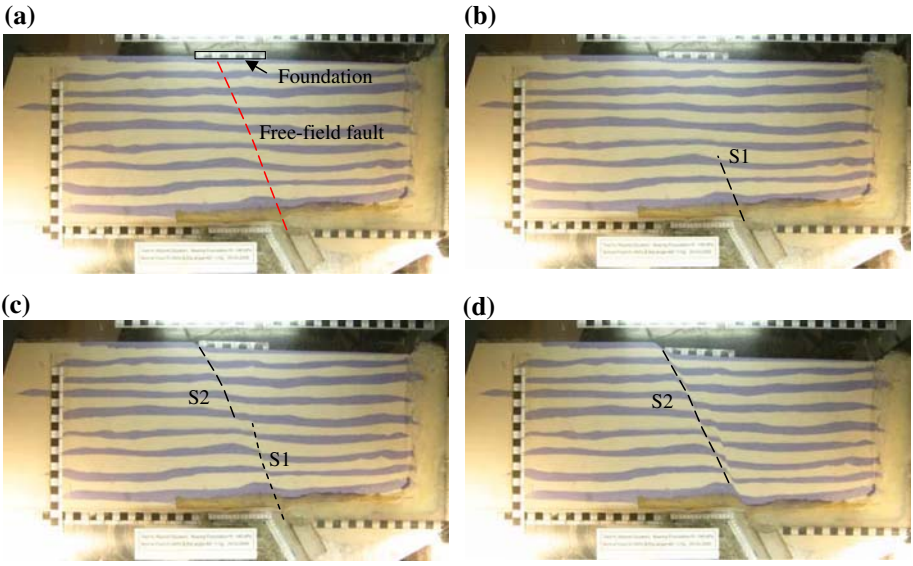

Fig. 7 Digital images taken during test 14 (B = 10 m; s = 3.0 m; q = 91 kPa) (**a**) Fault throw, h = 0.36 m (h_{model} = 3.2 mm). (**b**) h = 0.48 m (h_{model} = 4.1 mm) (**c**) h = 0.99 m (h_{model} = 8.6 mm) (**d**) h = 2.01 m (h_{model} = 17.5 mm)

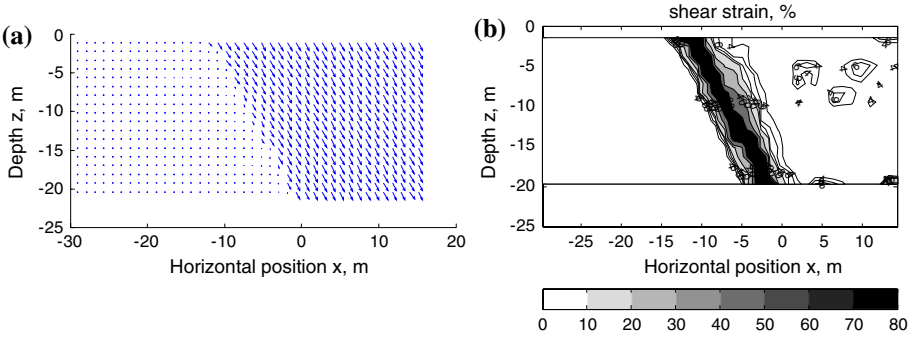

Fig. 8 Cumulative soil displacements after h = 2.01 m (h_{model} = 17.5 mm) in test 14 (**a**) Displacements (**b**) Maximum shear strain (γ_{max})

As for the free-field case, a fault propagates progressively upwards from the base. However, for this case there is a second main localisation which appears to propagate downwards from the displacement singularity of the left hand (foot wall) edge of the foundation ('S2' in Fig. 7c). The final fault rupture emergence was at the left of the foundation, so that the foundation caused a deviation of the fault position from the free-field case (by 3 m in this case). In addition, this final mechanism is not fully formed until h approaches 2 m (much greater fault displacement is required than with the free-field fault).

Although the final fault does not emerge beneath the foundation, significant rotation (θ), vertical (v) and horizontal (u) foundation movements are induced. Figure 9a plots the three components of foundation displacement against fault throw. The vertical and horizontal components of foundation rotation suggests that when fault throw, h > 0.5 m, the foundation moves downwards and laterally at the velocity of the hanging wall. This is confirmed by

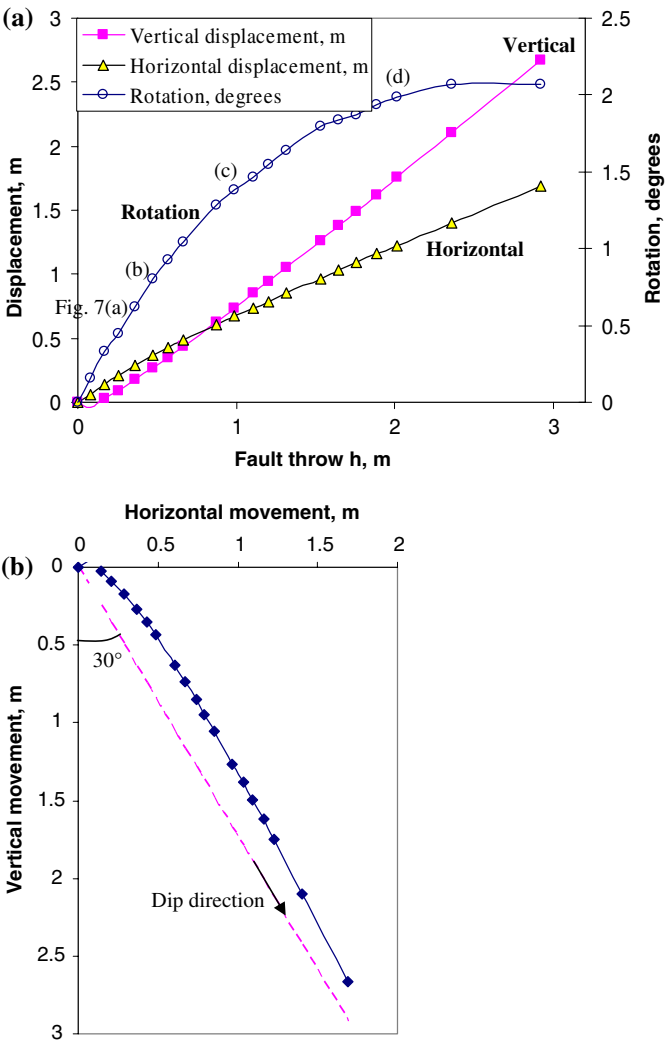

Fig. 9 Foundation displacement during test 14 (q = 91 kPa; B = 10 m; s = 3 m) (**a**) Foundation movements against faults throw (**b**) Foundation trajectory: horizontal *versus* vertical displacement

plotting the trajectory of foundation displacement in Fig. 9b (where the dashed line corresponds to the hanging wall displacements if it moves at the prescribed dip angle). However, the foundation rotation shows a different pattern with fault displacement. For fault throws, $h < 0.5$ m, the foundation rotates about 2° per metre of fault displacement ($\theta B/h \approx 0.35$, where foundation rotation, θ is in radians). However, when fault displacement, $h > 2$ m there is no further foundation rotation—the foundation translates downwards on the hanging wall and this is consistent with the mechanism shown in Fig. 8. This suggests that the fault deviation has successfully prevented any further foundation damage once the final mechanism has been mobilised. This agrees with observations from field case histories (e.g. Anastasopoulos and Gazetas 2007a; Faccioli et al. 2008) where heavy buildings appeared to deviate the fault displacements without significant damage.

Although the test confirms that fault deviation is possible due to the presence of shallow foundations, the reason cannot be deduced from a single test. Consequently further tests were carried out to investigate whether the deviation was due to the bearing pressure of the foundation (which adds input work to the system when displaced downwards and changes the stress field in the soil) or the kinematic restraint of the relatively rigid foundation. In addition, further tests were required to investigate other possible design conditions and create a database of observations for future numerical modelling.

4.3 Effect of footing bearing pressure, q on fault–foundation interaction

Test 15 was identical to test 14 except that the bearing pressure was reduced from 91 kPa to 37 kPa to examine the effect of the bearing pressure on the fault–foundation interaction. This bearing pressure could be considered to be appropriate for a 3 to 4-storey concrete building with a raft foundation.

The digital images captured during the test reveal that after an initial 'elastic' deformation with no localisation, a first localisation forms ('S1' on Fig. 10a) as for the heavier foundation. However, this localisation propagates almost three-quarters of the way to the ground surface (compared to half way for the heavier foundation) before a second localisation ('S2' on Fig. 10b) propagates from the footing corner with further fault movement. Again, this fault propagates downwards to form a complete fault by a displacement, $h = 2.03$ m (Fig. 10c) and shear plane 'S1' is then inactive.

Although the final failure mechanisms for the lighter foundation is similar to that for the heavier foundation (a single strong discontinuity deviated 3 m to the left to the edge of the foundation) and the same fault movements are required before the increase in foundation rotation ceases ($d\theta/dh = 0$ when $h > 2.3$ m for both foundations), the lighter foundation experiences larger rotations (Fig. 11). When the final mechanism has formed ($h \approx 2.5$ m), the heavy foundation ($q = 91$ kPa) has experienced, $\theta = 2.0°$, whereas the lighter foundation ($q = 37$ kPa) has $\theta = 5.1°$. This latter rotation may cause considerable structural damage or even collapse.

The reduction of bearing pressure appears to make the foundation more liable to damage for the conditions investigated here, but both foundations are sufficient to deviate the final fault from beneath the foundation. The difference in initial fault propagation (and the consequent foundation rotation) may be because the lower stresses in the soil beneath the lightly loaded foundation inhibit the propagation of localisation 'S1' less than beneath the heavily loaded foundation (compare Figs. 10b and 7c).

4.4 Effect of footing rigidity (EI) on fault–foundation interaction

To examine whether it is the bearing pressure on the ground surface or the kinematic restraint of the foundation that controls primarily the fault–foundation interaction, test 22 was conducted with similar conditions to that of test 14 ($q = 91$ kPa, $B \approx 10$ m; $s \approx 3$ m) except that the foundation was flexible. This was achieved by loosely connecting a bundle of steel rods which were placed above a rubber base of breadth 82 mm (9.43 m at prototype scale). The rods allowed shear/bending deformation and yet provided the appropriate bearing pressure to the flexible rubber base and the soil beneath.

The images taken during flight (Fig. 12) reveal a response similar to that of the rigid foundation (test 14). An initial localisation ('S1' in Fig. 12a) forms at the base before a second localisation ('S2' in Fig. 12b) propagates downwards from the far corner of the foundation until it forms a continuous shear plane (Fig. 11c). As before, the final shear plane is deviated

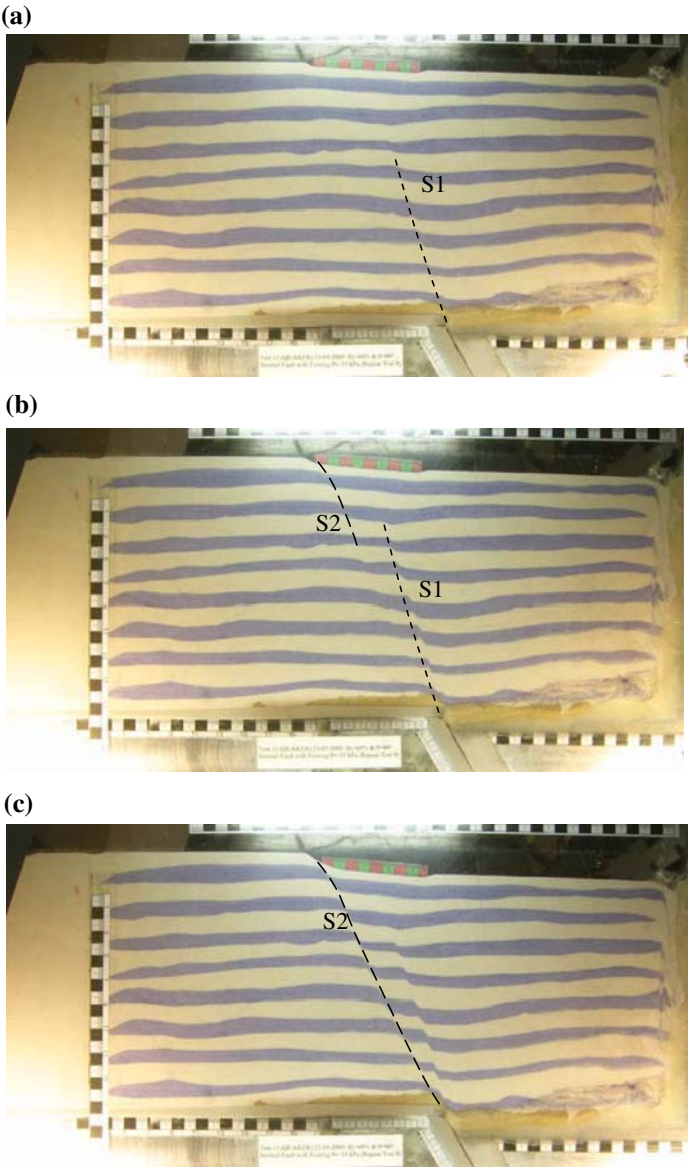

Fig. 10 Digital images captured during test 15 (q = 37 kPa; B = 10 m; s = 3 m) (**a**) h = 0.77 m (h_{model} = 6.7 mm) (**b**) h = 1.26 m (h_{model} = 11.0 mm) (**c**) h = 2.03 m (h_{model} = 17.7 mm)

3 m away from the hanging wall, just clipping the foot wall edge of the foundation. Again, the foundation experiences rotation (see Fig. 11) before mobilisation of the final mechanism (the single shear plane) after which time the foundation translates with the hanging wall giving no further rotation. The rotation angles plotted in Fig. 11 were calculated using a least squares, straight line fit to a plot of foundation settlement against position for each image taken (each corresponding to a different fault displacement) shown in Fig. 13. Figure 13 also shows that there was only a slight bending of the flexible foundation.

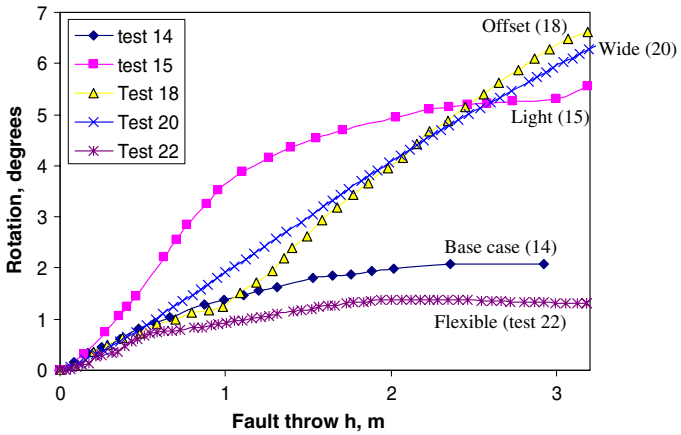

Fig. 11 Foundation rotation against fault throw (all tests)

The foundation rotation and soil localisation for the flexible foundation was qualitatively very similar to the rigid one for all magnitudes of fault throw investigated. However, the final rotation of the foundation was 1.4° for the flexible foundation compared to 2.0° for the rigid foundation. Some of this difference might be explained by the slight difference in foundation breadth (B = 10 m in test 14; B = 9.43 m in test 22) or because of the slight curvature of the flexible foundation.

The similarity between the results for the rigid and flexible foundations suggests that the kinematic restraint of the rigid foundation alone was not governing the location of the fault outcropping in the presence of the foundation—the fault could have outcropped through the flexible foundation but emerged on the footwall side. This suggests it is the foundation pressure which has cause the fault deviation (either in terms of additional work input to the system when displacing the foundation, or due to the increased stresses in the soil beneath the foundation). Further work is required to confirm this finding.

4.5 Effect of footing geometry (B, s) on fault-rupture–footing interaction

To examine the generality of the above results and to give additional test cases for validation of the accompanying numerical analysis (Anastasopoulos et al. 2008), two further centrifuge model tests were performed. In the first (test 18) the fault was placed B/2 further from the hanging wall, whilst in test 20 the foundation breadth, B was increased to 25 m (giving B/H = 1).

4.5.1 Effect of footing position

Four images captured during test 18 are shown in Fig. 14. As in previous tests, an initial steep localisation forms ('S1' in Fig. 14a), but with this foundation position, the shear plane extents to the surface by a displacement, h = 1.28 m (Fig. 14b) and appears to dip above the vertical near the soil surface (as observed by Cole and Lade 1984, albeit without a foundation). However, for a larger fault throw a second shear plane forms ('S2' in Fig. 14c) and the final image is shown in Fig. 14d.

The foundation rotation is plotted against fault throw in Fig. 11. When h < 1 m, the foundation response is similar to that for the equivalent foundation 5 m nearer the fault (test

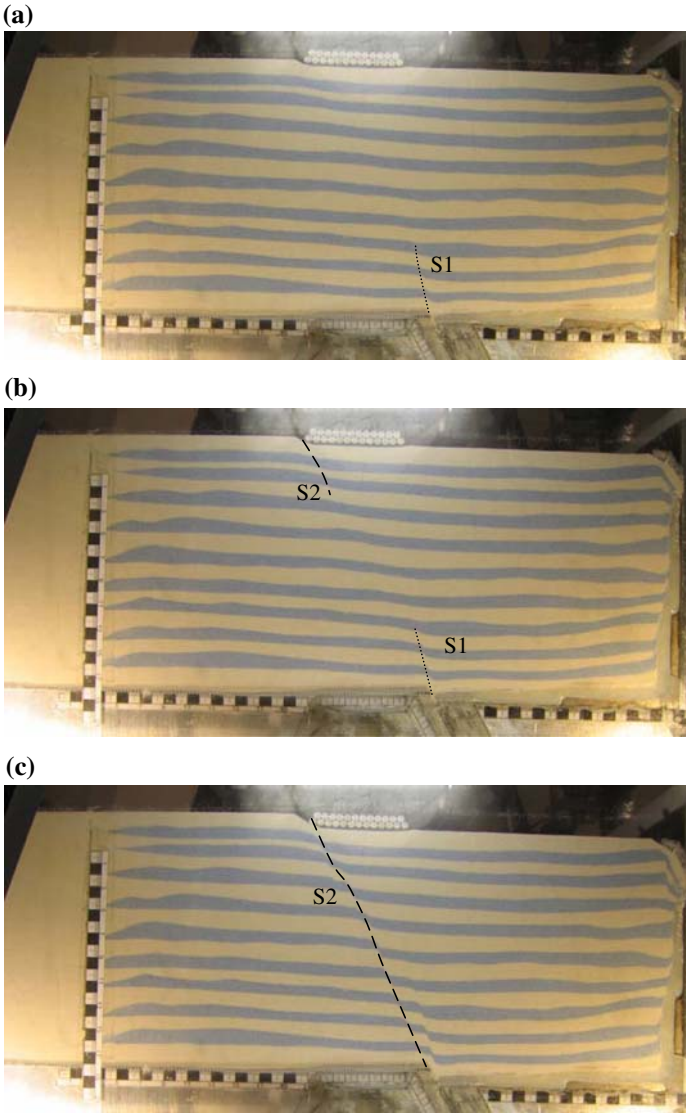

Fig. 12 Digital images captured during flexible foundation test (test 22, B = 9.43 m; s = 3.2 m; q = 91 kPa) (**a**) Fault throw, h = 0.63 m (h_{model} = 5.4 mm) (**b**) h = 0.81 m (h_{model} = 7.1 mm) (**c**) h = 1.52 m (h_{model} = 13.2 mm)

14). However, when h > 1 m, the foundation rotation increases more quickly with respect to fault displacement than previously and a 3 m fault throw produces a foundation rotation, $\theta = 6.4°$ (compared to $\theta = 2.1°$ when the foundation is 5 m closer to the fault) which is still increasing with fault throw. The fastest increase of foundation rotation with respect to increasing fault throw occurs with h = 1.4 m where rotation continues at approximately 3.4°/m (or $d\theta B/dh \approx 0.59$).

The difference in foundation response between tests 18 and 14 is that in test 18, the shear plane S1 continues to be active once shear plane S2 has formed and S2 is convex because

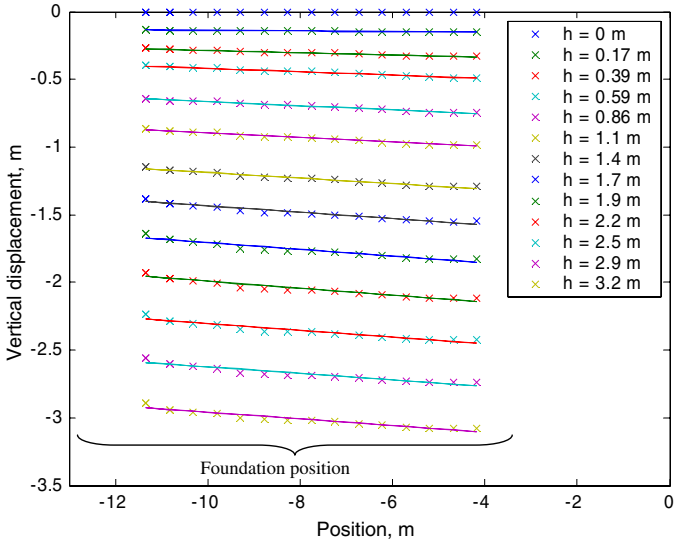

Fig. 13 Vertical settlement profile across the foundation during flexible foundation test (test 22)

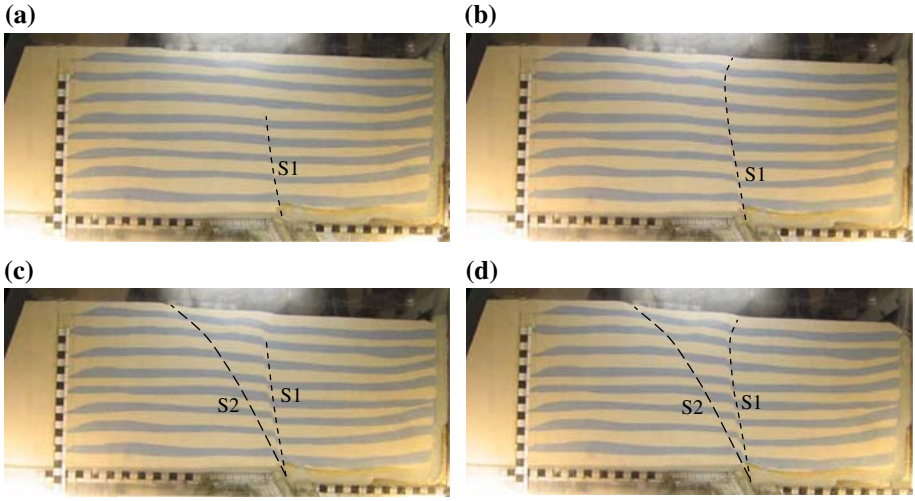

Fig. 14 Digital images captured during offset foundation test (test 18; B = 10 m; s = 8.3 m; q = 91 kPa) – foundation 5 m to the left of test 14 (**a**) Fault throw, h = 0.59 m (h_{model} = 5.1 mm) (**b**) h = 1.28 m (h_{model} = 11.2 mm) (**c**) h = 1.49 m (h_{model} = 13.0 mm) (**d**) h = 1.98 m (h_{model} = 17.2 mm)

of the large fault deviation required. Results from PIV from images taken at h = 1.37 m to h = 1.56 m (i.e. around the displacement for the image shown in Fig. 14c) are used to show the incremental displacement vectors (Fig. 15a) and incremental maximum shear strain contours (Fig. 15b) when $d\theta B/dh$ is greatest. The incremental deformation mechanism shown in Fig. 15 confirms that both S1 and S2 are active, but that there is little shear outside these zones. The block within the two shear planes is rotating clockwise and may also be subject to a small amount of shear. The foundation is resting on this block and thus also continues to rotate clockwise. This mechanism is facilitated by the weight of the foundation and might

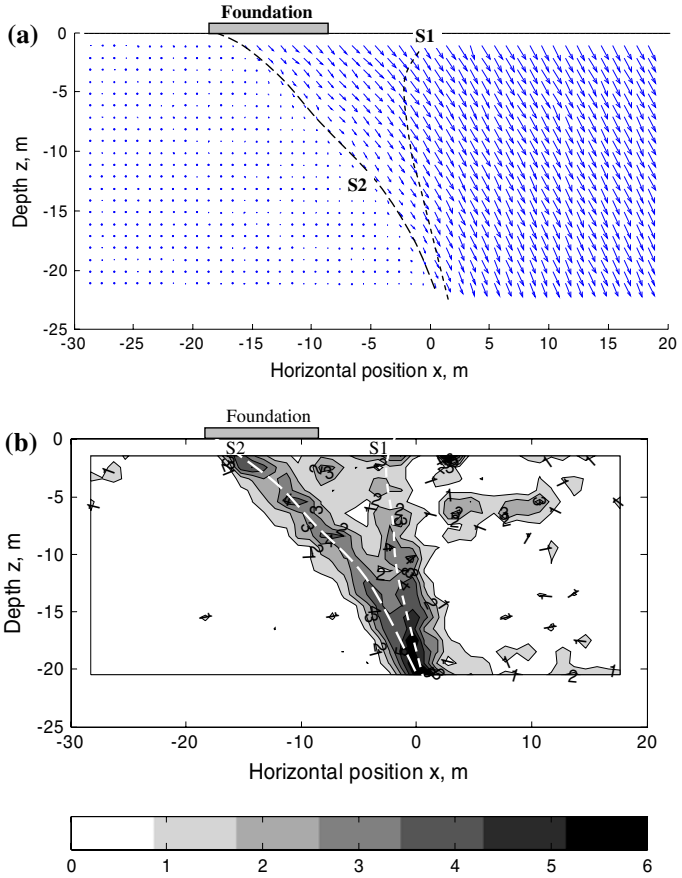

Fig. 15 Measured incremental soil displacements and shear strain for h = 1.37–1.56 m (Δh = 0.19 m) (h/H = 5.5%; Δh/H = 0.76%). Offset foundation (test 18) (**a**) Incremental displacement vectors (**a**) contours of incremental γ_{max}

be considered as a partial bearing capacity failure due to the reducing support of the hanging wall deformation mechanism S1.

The difference in both foundation and soil response between tests 14 and 18 has revealed that the position of the foundation will have significant influence on the interaction between the fault and the foundation. Further investigation is needed to study the response of foundations in a wide range of positions.

4.5.2 Footing breadth

For test 20, the foundation breadth, B = 25 m (B/H = 1) and the free-field fault position, s/B = 0.44. The results from this test can be compared with those from test 14 which had the same loading conditions but a narrower foundation B = 10 m (B/H = 0.4).

The digital images captured during test 20 are shown as Fig. 16. As in the previous tests, an initial steep localisation forms (Fig. 16a) before a second localisation is formed on the footwall (Fig. 16b) which finally propagates to the soil surface (Fig. 16d). The second localisation emerges at the ground surface just to the left of the foundation for the final mechanism

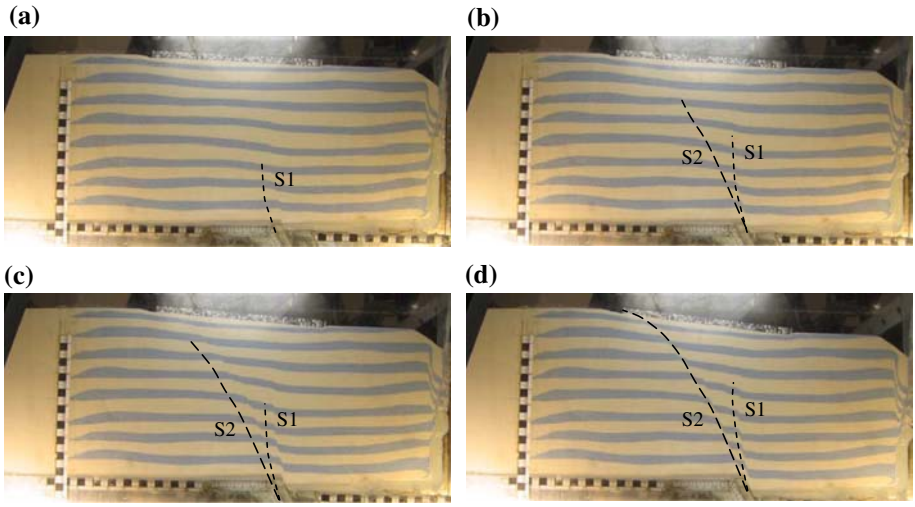

Fig. 16 Digital images captured during wide foundation test (test 20; B = 25 m; q = 91 kPa; s = 10.9 m) (**a**) Fault throw, h = 1.00 m (h_{model} = 8.7 mm) (**b**) h = 1.52 m (h_{model} = 13.2 mm) (**c**) h = 1.99 m (h_{model} = 1.73 mm) (**d**) h = 3.04 m

with a very low dip angle near the foundation corner. This involves a 10.9 m deviation of the fault towards the foot wall from the free-field case. The response differs also to that of test 14 because larger fault throws are required to propagate the shear planes: h = 1 m for appreciable mobilisation of S1 (Fig. 16a); h ≈ 2 m to propagate S2 to the soil surface (Fig. 16c).

Incremental soil deformations calculated using PIV are shown in Fig. 17 for h ≈ 1.9 m (Fig. 17a, b) and h ≈ 3 m (Fig. 17c, d). Both shear planes are clearly active when h ≈ 1.9 m with S1 undergoing more shear strain than S2 (Fig. 17b). By a fault throw, h ≈ 3 m, Fig. 17d shows that shear plane S1 is almost inactive and that nearly all fault displacement is taken up in shear plane S2.

The rotational response of the foundation (Fig. 11) shows that the foundation rotation is increasing even when h = 3 m. At this stage, the single shear plane ('S2' in Fig. 16d) is not simply dividing a rigidly translating hanging wall (with the foundation resting on it) from the footwall as in the previous tests. Instead, deformation of the soil beneath the foundation or elsewhere on the hanging wall due to the convexity of the localisation must provoke continuous foundation rotation.

5 Discussion and implications for design

The results of the centrifuge model tests have confirmed the findings of field observations: heavily loaded foundations can deviate earthquake faults away from the foundations. Hence, it is possible to design foundations that will not undergo damage due to fault rupture under such conditions.

For the case of normal faulting, the fault deviation appears to be due to the bearing pressure rather than the kinematic restraint of the foundations: a flexible foundation behaved almost identically to a rigid foundation. The bearing pressure will increase stresses in the soil beneath

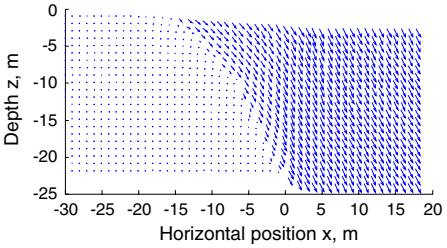

(a) Incremental displacement vectors from h = 1.74 m to h = 1.99 (Δh = 0.25)

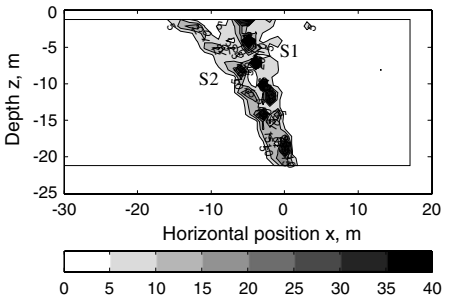

(b) Contours of incremental γ_{max} for h = 1.74 m to h = 1.99 (Δh = 0.25)

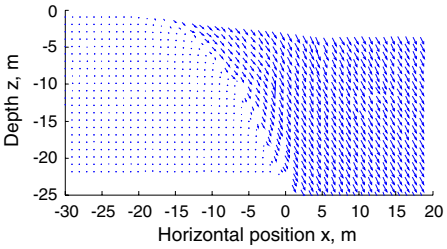

(c) Incremental displacements for h = 2.83 m to 3.04 m. (Δh = 0.21 m)

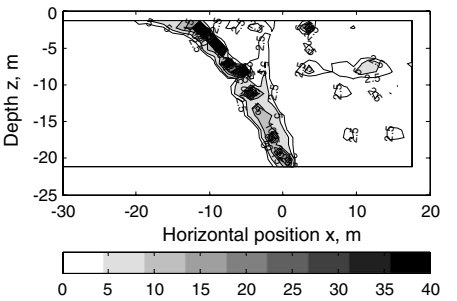

(d) Contours of incremental γ_{max} for h = 2.83 m to 3.04 m. (Δh = 0.21 m)

Fig. 17 Incremental displacement vectors and shear strain contours during the wide foundation test (test 20) (**a**) Incremental vectors from h = 1.74 m to h = 1.99 (Δh = 0.25) (**b**) Contours of incremental γ_{max} for h = 1.74 m to h = 1.99 (Δh = 0.25) (**c**) Incremental displacements for h = 2.83 m to 3.04 m (Δh = 0.21 m) (**d**) Contours of incremental γ_{max} for h = 2.83 m to 3.04 m (Δh = 0.21 m)

both increasing shear strength and stiffness and suppressing dilation. In addition, downwards displacement of the foundation adds input work to the system and thus mechanisms which cause foundation settlement (such as deviation of the fault to the footwall side of the foundation) are advantaged.

The results shown here have shown that the interaction between the faults and the foundation is subtle and sensitive to the foundation breadth, bearing pressure and position relative to the fault. All foundations investigated in this test series deviated the fault emergence from beneath the foundation, but each foundation underwent different amounts of (generally rigid body) rotation. This rotation may be enough to damage or destroy the supported structures.

For design is it is expected that single narrow heavily loaded foundations are more likely to deflects faults, but a number of isolated individual foundations supporting a structure may lead to rupture between foundations. A wide raft foundation may gently smooth out the fault displacements but a significant depth of soil is needed compared to the foundation width to deflect a fault. Further investigation is required to understand the phenomena sufficiently to develop general design methods.

Finite element analysis may prove an effective design tool. However, this requires the development of robust, yet accurate numerical approaches. The data herein can be used to validate such numerical modelling.

6 Conclusions

The interaction between normal faulting and shallow foundations in drained soils has been investigated for the first time in the geotechnical centrifuge. A series of model tests combined with digital image analysis has found that:

- The propagation of a fault in free-field conditions was similar to that observed by previous researchers. There was progressive localisation of shear deformation from the base of the soil layer up to the ground surface. Once this localisation reached the soil surface, there was no further deformation of the soil remote from the shear plane.
- Heavily loaded foundations deviated earthquake faults away from the foundations, thus confirming field observations.
- A flexible foundation was also able to deviate the earthquake fault suggesting that it was the bearing pressure, not the kinematic restraint of the rigid foundation that caused the fault rupture deviation.
- Despite deviating the faults, all foundations underwent significant rotation whilst the final fault-rupture mechanism was developing. This rotation appeared to be reduced with increasing bearing pressures.
- For most of the foundations investigated, the fault deviated to the footwall side of the foundation, and once the fault throw was large enough to propagate this rupture to the ground surface, this resulted in no further rotation of the foundation. The foundation simply translated rigidly on the hanging wall which was displacing at the dip angle. However, this did not occur when the footwall edge of the foundation was far from the base discontinuity. This required a final fault with a low dip angle (and a convex shear plane) which provoked continued foundation displacement even for large fault throws.
- Finally, the position of the fault relative to the foundation appeared critical to the interaction response. Hence, a range of possible fault positions should be considered in design if the fault position is uncertain.

Acknowledgements The work forms part of the project "Fault-rupture and strong shaking effects on the safety of composite foundations and pipeline systems: Quantification and Reduction of Seismic Risk Through the Application of Advanced Geotechnical Engineering Techniques" (QUAKER). This was funded by the European Commission under contract number EVG1-CT 2002-00064. We are also grateful for technical discussion with our QUAKER colleagues throughout the project. Finally, the authors would like to thank Dr. White (Cambridge University) and Dr. Take (Queen's University) for the use of the Cambridge Geo-PIV program.

References

Anastasopoulos I, Gazetas G (2007a) Foundation-structure systems over a rupturing normal fault: I. Observations after the Kocaeli 1999 Earthquake. Bull Earthquake Eng 5(3):253–275. doi: 10.1007/s10518-007-9029-2

Anastasopoulos I, Gazetas G (2007b) Behaviour of structure-foundation systems over a rupturing normal fault: II. Analyses, experiments, and the Kocaeli case histories. Bull Earthquake Eng 5(3):277–301. doi:10.1007/s10518-007-9030-9

Anastasopoulos I, Callerio A, Bransby MF, Davies MCR, Gazetas G, Masella A et al (2008) Numerical analyses of fault–foundation interaction. Bull Earthquake Eng (submitted)

Berill JB (1983) Two-dimensional analysis of the effect of fault rupture on buildings with shallow foundations. Soil Dyn Earthquake Eng 2(3):156–160. doi:10.1016/0261-7277(83)90012-8

Bolton MD (1986) The strength and dilatancy of sands. Geotechnique 36(1):65–78

Bray JD (1990) The effects of tectonic movements on stresses and deformations in earth embankments. Ph.D. Dissertation, University of California, Berkeley

Bray JD (2001) Developing mitigation measures for the hazards associated with earthquake surface fault rupture. In A workshop on seismic fault-induced failures—possible remedies for damage to urban facilities. Japan Society for the promotion of science, University of Tokyo, Japan, January 11–12, pp 55–79

Bray JD, Seed RB, Cluff LS, Seed HB (1994) Earthquake fault rupture propagation through soil. J Geotech Eng, ASCE 120(3):543–561

Cole DA Jr, Lade PV (1984) Influence zones in alluvium over dip-slip faults. J Geotech Eng 110:599–615

Faccioli E, Anastasopoulos I, Callerio A, Gazetas G (2008) Case histories of fault–foundation interaction. Bull Earthquake Eng (submitted)

Gaudin C (2002) Modélisation physique et numérique des écrans de soutènement: application à l'étude de l'effet d'une surcharge sur le sol soutenu. PhD. thesis, Université de Nantes.

Lade PV, Cole DA, Cummings D (1984) Multiple failure surfaces over dip-slip faults. J Geotech Eng 110(5):616–627

Lazarte CA, Bray JD (1996) A study of strike-slip faulting using small-scale models. Geotech Test J, Am Soc Test Mater 19(2):118–129

Lazarte CA (1996) The response of earth structures to surface fault rupture. Ph.D. Thesis, Department of Civil Engineering, University of California, Berkeley

Muhlhaus HB, Vardoulakis L (1987) The thickness of shear bands in granular materials. Geotechnique 37(3):271–283

Muir Wood D, Stone KJL (1994) Some observations of zones of localisation in model tests on dry sand. In: Chambon R, Desrues J, Vardoulakis I (eds) Localisation and bifurcation theory for soils and rocks. A.A. Balkema, Rotterdam, pp 155–164

Muir Wood D (2002) Some observations of volumetric instabilities in soils. Int J Solids Struct 39:3429–3449

Muir Wood D (2004) Geotechnical modelling. Spon Press, London

Niccum MR, Cluff LS, Chamoro F, Wylie L (1976) Banco Central de Nicaragua: a case history of a high-rise building that survived surface fault rupture. In Humphrey CB (ed) Engineering Geology and Soils Engineering Symposium, No. 14. Idaho Transportation Department, Division of Highways, pp 133–144

O'Rourke MJ (2003) Buried pipelines. In: Chen W-F, Scawthorn C (eds) Earthquake engineering handbook. CRC Press, Boca Raton

Pamuk A, Kalkanb E, Linga HI (2005) Structural and geotechnical impacts of surface rupture on 468 highway structures during recent earthquakes in Turkey. Soil Dyn Earthquake Eng 25:581–589. doi:10.1016/j.soildyn.2004.11.011

Pecker A, Faccioli E, Gazetas G, Paolucci R (2008), Design recommendations for fault–foundation interaction. Bull Earthquake Eng (submitted)

Roth WH, Scott RF, Austin I (1981) Centrifuge modelling of fault propagation through alluvial soils. Geophys Res Lett 8(6):561–564. doi:10.1029/GL008i006p00561

Roth WH, Sweet J, Goodman RE (1982) Numerical and physical modelling of flexural slip phenomena and potential for fault movement. Rock Mech (Suppl. 12):27–46

Scarpelli G, Wood DM (1982) Experimental observations of shear band patterns in direct shear. In: Vermeer PA, Luger HJ (eds) Proceedings of the IUTAM symposium on deformation and failure of granular materials. Balkema, Rotterdam, pp 473–484

Schofield AN (1980) Cambridge University geotechnical centrifuge operations. Rankine lecture. Geotechnique 30(3):227–268

Scott RF, Schoustra JJ (1974) Nuclear power plant siting on deep alluvium. J Geotech Eng Div ASCE 100(4):449–459

Stone KJL, Muir Wood D (1992) Effects of dilatancy and particle size observed in model tests on sand. Soils Found 32(4):43–57

Ulusay R, Aydan O, Hamada M (2002) The behaviour of structures built on active fault zones: examples from the recent earthquakes of Turkey. Struct Eng Earthquake Eng, JSCE 19(2):149–167.

Vardoulakis I, Graf B, Gudehus G (1981) Trap-door problem with dry sand: a statical approach based on model test kinematics. Int J Numer Anal Methods Geomech 5:58–78. doi:10.1002/nag.1610050106

White RJ, Stone KJL, Jewel RJ (1994), Effect of particle size on localization development in model tests on sand. In: Leung, Lee, Tan (eds) Centrifuge 94. Balkema, Rotterdam, pp 817–822

White DJ, Take WA, Bolton MD (2003) Soil deformation measurement using particle image velocimetry (PIV) and photogrammetry. Geotechnique 53(7):619–631. doi:10.1680/geot.53.7.619.37383

Yilmaz MT, Paolucci R (2006) Earthquake fault rupture–shallow foundation interaction in undrained soils: a simplified analytical approach. Earthquake Eng Struct Dyn 36(1):101–118